

RELATION BETWEEN STRAIN HARDENING OF STEEL AND CRITICAL IMPACT VELOCITY IN TENSION

This paper is dedicated to our friend, Prof. Janusz Roman Klepaczko who passed away in August 15, 2008, for his pioneer contributions to the understanding of the Critical Impact Velocity phenomenon

JOSÉ A. RODRÍGUEZ-MARTÍNEZ

University Carlos III of Madrid, Department of Continuum Mechanics and Structural Analysis, Madrid, Spain; e-mail: jarmarti@ing.uc3m.es

ALEXIS RUSINEK

Engineering School of Metz (ENIM), Laboratory of Mechanics, Biomechanics, Polymers and Structures(LaBPS), Metz, France; e-mail: rusinek@enim.fr

ANGEL ARIAS

University Carlos III of Madrid, Department of Continuum Mechanics and Structural Analysis, Madrid, Spain

In the present paper, a numerical study on the influence of strain hardening on the Critical Impact Velocity (CIV) in tension is conducted. Finite element code ABAQUS/Explicit is used to carry out numerical simulations of dynamic tension tests in a wide range of impact velocities up to that corresponding to the CIV. The constitutive relation due to Rusinek and Klepaczko (2001) has been used to define the material behaviour. Strain hardening parameters of the RK model were varied during the simulations. Numerical results are compared with those obtained from the analytical description of CIV proposed by Klepaczko (2005). Satisfactory agreement is found between numerical and analytical approaches. The analysis allows for a better understanding of the causes responsible of the CIV appearance.

Key words: critical impact velocity, RK model, dynamic tension

1. Introduction

The study of materials subjected to extreme loading conditions like crash, impact or explosion, is of considerable interest in different industrial fields. A relevant amount of publications can be found in the international literature dealing with high strain rate behaviour of metallic materials related with

different engineering applications (Arias *et al.*, 2008; Borvik *et al.*, 2002; Forrestal and Piekutowski, 2000; Klepaczko, 2006; Klepaczko and Klosak, 1999; Klepaczko *et al.*, 2009; Nemat-Nasser and Guo, 2003; Rusinek and Klepaczko, 2003; Rusinek *et al.*, 2005).

When metals are subjected to impulsive loads, the effects of strain hardening, strain rate and temperature sensitivity play the main role in the behaviour of a material. Moreover, the thermal coupling cannot be ignored at high strain rates (Klepaczko, 2005). The heat energy due to plastic deformation cannot be transmitted and the material behaves under an adiabatic condition of deformation. Such a condition induces localization of deformation which is a precursor of failure. In addition, in dynamic problems, the propagation of elastic and plastic waves that, depending on the initial boundary value problem, could totally govern the response of the material is observed (Rusinek *et al.*, 2005, 2008).

An example of an initial boundary value problem which is ruled by the plastic wave effect is the phenomenon called Critical Impact Velocity (CIV). This phenomenon takes place when the speed of plastic waves reaches zero due to localization of plastic deformation in adiabatic conditions. Thus, the existence of CIV for metals imposes the upper limit to the dynamic tension test for determination of material properties. Loading conditions corresponding to CIV could be reached in some industrial processes like fast cutting, high speed machining or ballistic impact.

The CIV is considered as a material property (Clark and Wood, 1950; Klepaczko, 2005; Mann, 1936). Such a conclusion was reported for the first time by Mann (1936). In that study, tension impact tests revealed that the maximum energy absorbed by a specimen was well defined for a certain impact velocity independently of length of the specimen. Later, Clark and Wood (1950) confirmed experimentally the existence of CIV in tension. Different specimen lengths were tested in a wide range of impact velocities. The conclusion was analogous to that previously achieved by Mann (1936).

However, the value of CIV in tension may suffer considerable variations depending on the material considered. Such a conclusion was drawn by Hu and Daehn (1996) estimating analytically CIV in tension for several materials, Fig. 1.

The normalized material density ρ_n introduced in Fig. 1 is the ratio of the density to the constant $\rho_n = \rho/K$ where $\bar{\sigma} = K \cdot (\bar{\epsilon}^p)^n$.

There are not many studies dealing with the influence of thermo-viscoplastic behaviour of the material on the CIV value. There are not many materials with an identified CIV in tension. Moreover, up to now, the cau-

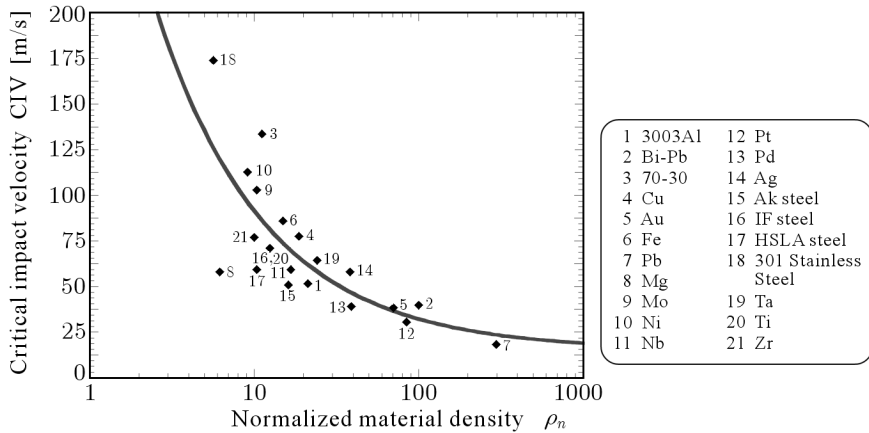


Fig. 1. Estimation of CIV in tension for different materials (Hu and Daehn, 1996);
 $CIV = A + B\rho_n^{-C}$, $A = 15.175$, $B = 342.2$, $C = 0.65102$

ses which are behind the CIV value exhibited by each particular material are hardly known. Such lack of information is due to different causes:

- The experiments required to identify CIV are sophisticated and need expensive technical resources.
- The analytical estimations of CIV may be subjected to strong assumptions. Such assumptions may considerably modify the results obtained from the analytical description of the process. This problem will be examined ahead in the present paper.

Numerical methods have recently become of relevance in analysing the CIV problem (Klosak *et al.*, 2001; Rusinek *et al.*, 2005). In the present paper, the FE code ABAQUS/Explicit is used to conduct numerical simulations of fast tension tests. The application of FE analysis allows to determine the relevance of different aspects of the material behaviour on the CIV value. Using FE simulations, the time and cost required to obtain results for a particular problem are reduced in comparison with experiments. In the present paper, the constitutive relation due to Rusinek and Klepaczko (2001) (RK model) is used to define the material behaviour. Strain hardening parameters of the RK model are varied during simulations. Their influence on the CIV value is evaluated. The analysis is conducted for a wide range of impact velocities up to that corresponding to the CIV. Numerical results are compared with those obtained from the analytical description proposed by Klepaczko (2005). The analysis allows for a better understanding of the causes responsible of the CIV appearance.

2. The Rusinek-Klepaczko model

The RK is a physical-based model founded on the additive decomposition of stress $\bar{\sigma}$ (Klepaczko, 1975; Kocks *et al.*, 1975; Seeger, 1957). Thus, the total stress is an addition of two terms σ_μ and σ^* , which define the strain hardening and thermal activation processes, respectively, Eq. (2.1)₁. The first one is called the internal stress and the second one, the effective stress. The multiplicative factor $E(T)/E_0$ defines Young's modulus evolution with temperature, Eq. (2.1)₂ (Klepaczko, 1998a)

$$\begin{aligned} \bar{\sigma}(\bar{\varepsilon}_p, \dot{\bar{\varepsilon}}_p, T) &= \frac{E(T)}{E_0} [\sigma_\mu(\bar{\varepsilon}_p, \dot{\bar{\varepsilon}}_p, T) + \sigma^*(\dot{\bar{\varepsilon}}_p, T)] \\ E(T) &= E_0 \left\{ 1 - \frac{T}{T_m} \exp \left[\theta^* \left(1 - \frac{T}{T_m} \right) \right] \right\} \quad T > 0 \end{aligned} \quad (2.1)$$

where E_0 , T_m and θ^* denote Young's modulus at $T = 0$ K, the melting temperature and the characteristic homologous temperature, respectively. The constant θ^* defines thermal softening depending on the crystal lattice of the material (Rusinek *et al.*, 2009).

The effective stress is defined as follows

$$\sigma^*(\dot{\bar{\varepsilon}}^p, T) = \sigma_0^* \left\langle 1 - D_1 \left(\frac{T}{T_m} \right) \log \frac{\dot{\bar{\varepsilon}}^{max}}{\dot{\bar{\varepsilon}}^p} \right\rangle^{m^*} \quad (2.2)$$

where σ_0^* is the effective stress at $T = 0$ K, D_1 is the material constant, $\dot{\bar{\varepsilon}}^{max}$ is the maximum strain rate accepted for a particular analysis and m^* is a constant allowing one define the strain rate-temperature dependency (Klepaczko, 1987).

The internal stress is defined by the plasticity modulus $B(\dot{\bar{\varepsilon}}^p, T)$ and the strain hardening exponent $n(\dot{\bar{\varepsilon}}^p, T)$ which are dependent on the strain rate and temperature

$$\sigma_\mu(\bar{\varepsilon}^p, \dot{\bar{\varepsilon}}^p, T) = B(\dot{\bar{\varepsilon}}^p, T) (\varepsilon_0 + \bar{\varepsilon}^p)^{n(\dot{\bar{\varepsilon}}^p, T)} \quad (2.3)$$

The explicit formulation describing the modulus of plasticity is given by

$$B(\dot{\bar{\varepsilon}}_p, T) = B_0 \left(\frac{T}{T_m} \log \frac{\dot{\bar{\varepsilon}}^{max}}{\dot{\bar{\varepsilon}}_p} \right)^{-\nu} \quad (2.4)$$

where B_0 is a material constant, ν describes temperature sensitivity and $\dot{\bar{\varepsilon}}^{max}$ is the maximum strain rate validated for this model.

The strain hardening exponent is defined as follows

$$n(\dot{\bar{\varepsilon}}_p, T) = n_0 \left\langle 1 - D_2 \left(\frac{T}{T_m} \right) \log \frac{\dot{\bar{\varepsilon}}_p}{\dot{\varepsilon}_{min}} \right\rangle \quad (2.5)$$

where n_0 is the strain hardening exponent at $T = 0\text{K}$, D_2 is the material constant and $\dot{\varepsilon}^{min}$ is the minimum strain rate validated for this model.

In the case of adiabatic conditions of deformation, the approximation of thermal softening of the material via adiabatic heating is given by

$$\Delta T_{ad} = \frac{\beta}{\rho C_p} \int_{\varepsilon^e}^{\bar{\varepsilon}^p} \sigma(\xi, \dot{\bar{\varepsilon}}^p, T) d\xi \quad (2.6)$$

where β is the Taylor-Quinney coefficient, ρ is the material density and C_p is the specific heat at a constant pressure. Transition from isothermal to adiabatic conditions is assumed at $\dot{\bar{\varepsilon}}_p = 10\text{s}^{-1}$, in agreement with experimental observations and numerical estimations (Berbenni *et al.*, 2004; Oussouaddi and Klepaczko, 1991; Rusinek *et al.*, 2007).

On the basis of model calibration for DH-36 steel reported in Klepaczko *et al.* (2009), two material constants of the RK model are varied, n_0 and B_0 , see Table 1. The range of variation of these parameters is given in Table 1. The material parameters remained constant during simulations are listed in Table 2.

Table 1. Parameters of the RK model varied during analytical and numerical analysis

n_0 [-]	B_0 [MPa]
0.1, 0.2, 0.3, 0.4	750, 1250, 1750, 2250

Table 2. Parameters of the RK model assumed constant

D_2 [-]	σ_0^* [MPa]	m^* [-]	ν [-]	D_1 [-]	E_0 [GPa]	θ^* [-]	T_m [K]	C_p [J/kg·K]	β [-]	ρ [kg/m ³]
0.05	500	2	0.02	0.5	200	0.7	1600	470	0.9	7800

The constitutive relation has been implemented in ABAQUS/Explicit via a user subroutine using the implicit consistent algorithm proposed by Zaera and Fernandez-Saez (2006).

In the following section, the configuration used to conduct numerical simulations is described.

3. Numerical configuration and validation

Geometry and dimensions of the specimen used are based on a previous work (Rusinek *et al.*, 2005). Such geometry of the specimen allows for observing well developed necking (Rusinek *et al.*, 2005). A scheme of the specimen is shown in Fig. 2. The thickness of the sample is $t_s = 1.65$ mm. Its impacted side is subjected to a constant velocity during the simulation. The movements are restricted to the axial direction. The opposite impact side is embedded. Such configuration idealizes boundary conditions required for the test. It must be noted that during experiments it might be difficult to obtain such an arrangement (*the applied velocity may not be constant during the whole test, transversal displacements of the specimen may occur*). However, this numerical configuration is suitable to impose a constant level of deformation rate on the active part of the specimen during the simulations.

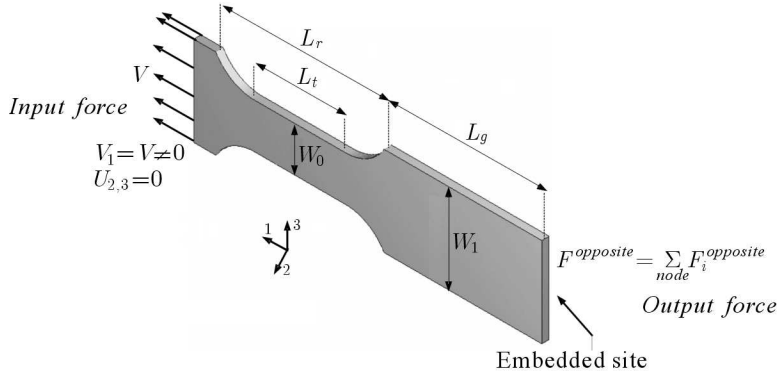


Fig. 2. Geometry and dimensions [mm] of the specimen used during simulations; $L_g = 36$ mm, $L_r = 37$ mm, $L_t = 20$ mm, $W_0 = 10$ mm, $W_1 = 20$ mm

The active part of the specimen has been meshed using hexahedral elements whose aspect ratio was close to $1 : 1 : 1$ ($\approx 0.5 \times 0.5 \times 0.5$ mm³). This definition is in agreement with the considerations reported by Zukas and Scheffler (2000). Beside the active part of the specimen two transition zones are defined. These zones are meshed with tetrahedral elements, Fig. 3. Such transition zones allow for increasing the number of elements along the 3 axis of the specimen, Fig. 3. This technique is used to get hexahedral elements in the outer sides of the sample maintaining the desired aspect ratio $1 : 1 : 1$.

The boundary conditions applied to simulations must guarantee the tensile state in the active part of the specimen. In Fig. 3a, triaxiality contours during the numerical simulation are shown. It can be observed that the triaxiality

value in the active part of the specimen is that corresponding to the tension state $\sigma_{triaxiality} = 0.33$.

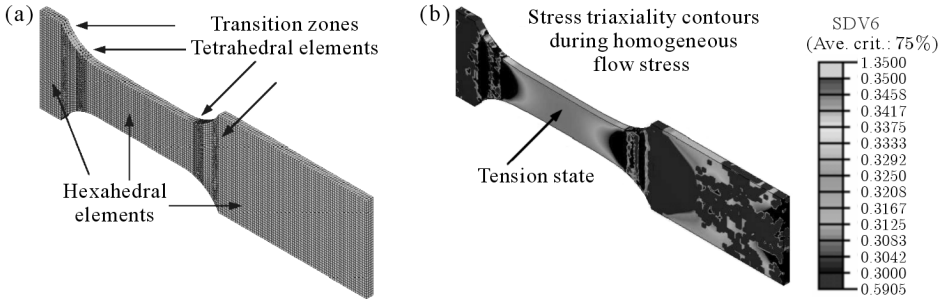


Fig. 3. (a) Mesh configuration used during numerical simulations. (b) Numerical estimation of the triaxiality contours

For validation of the numerical approach, a comparison between the analytical predictions of the model and the numerical results is conducted in terms of true stress along with plastic strain, Fig. 4. It can be seen that the numerical results fit the analytical predictions of the model. The oscillation obtained in the numerical values is caused by the elastic wave propagation. It is dissipated along the loading time due to spread of plasticity in the active part of the specimen, Fig. 4.

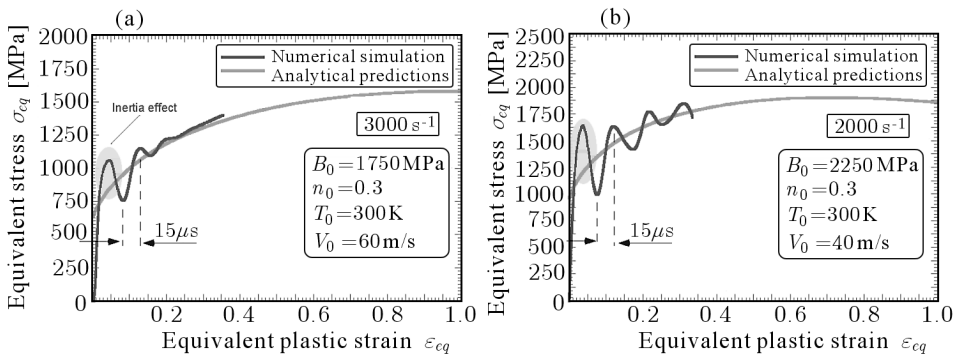


Fig. 4. Comparison of the analytical predictions with numerical results (elastic wave propagation: $C_0 = \sqrt{E(T)/\rho} = 5200 \text{ m/s}$, $15 \mu\text{s} \rightarrow 78 \text{ mm} = \text{length specimen}$)

In the following section, the influence of the main strain hardening parameters on CIV in tension is analysed.

4. Analysis and results

The first results reported are those corresponding to the variation of the parameter n_0 .

4.1. Effect of the strain hardening exponent n_0

Analytical predictions of the RK model in terms of flow stress along with strain for several values of n_0 are shown in Fig. 5. It can be observed that the strain hardening $d\bar{\sigma}/d\bar{\varepsilon}_p$ strongly increases with n_0 , Fig. 5b. However, the yield stress level is considerably diminished, Fig. 5a. The condition of instability $d\bar{\sigma}/d\bar{\varepsilon}_{neck} = \bar{\sigma}$ (Considere, 1885) is revealed as highly dependent on the strain hardening exponent n_0 . The augmentation of strain hardening delays the appearance of instabilities, increasing ductility of the material, Fig. 5c. In Fig. 5d it is shown that at a high rate of deformation the instability strain ε_{neck} remains constant. Such a conclusion is in agreement with the observations reported in Rusinek and Zaera (2007). The condition of trapping of plastic deformation $d\bar{\sigma}/d\bar{\varepsilon}_p = 0 \rightarrow C_p = 0$, is analysed in Fig. 5e. Since the strain hardening increases with n_0 , the plastic wave speed also does it. Notable differences in the value of the strain corresponding to $C_p = 0$ condition are predicted for different values of n_0 . Due to these considerations, great influence of the strain hardening exponent n_0 on the CIV value can be expected.

These expectations are fulfilled in sight of the numerical results shown in Fig. 6, where equivalent plastic strain contours are shown for two different impact velocities ($V_0 = 120$ m/s and $V_0 = 100$ m/s) and several values of n_0 . For both impact velocities, in the case of $n_0 = 0.1$, the deformation is localised close to the impact end, Fig. 6. The CIV is reached. On the contrary, in the case of $n_0 = 0.4$, the necking takes place in the middle, in one case ($V_0 = 120$ m/s), and in the opposite impact side, in another case ($V_0 = 100$ m/s), Fig. 6e-h. In those last cases, the plastic deformation is spread along the whole active part of the specimen.

In Fig. 8, the equivalent strain rate contours estimated by numerical simulations is shown. In the case of $n_0 = 0.1$, the strain rate level is not uniform along the active part of the specimen, Fig. 8a-c. A high level of the deformation rate is instantaneously reached after the impact in the zone where the necking takes place, Fig. 8a. In the case of $n_0 = 0.4$, once inertia effects are dissipated, the strain rate level along the active part of the specimen remains constant until the necking appears, Fig. 8d.

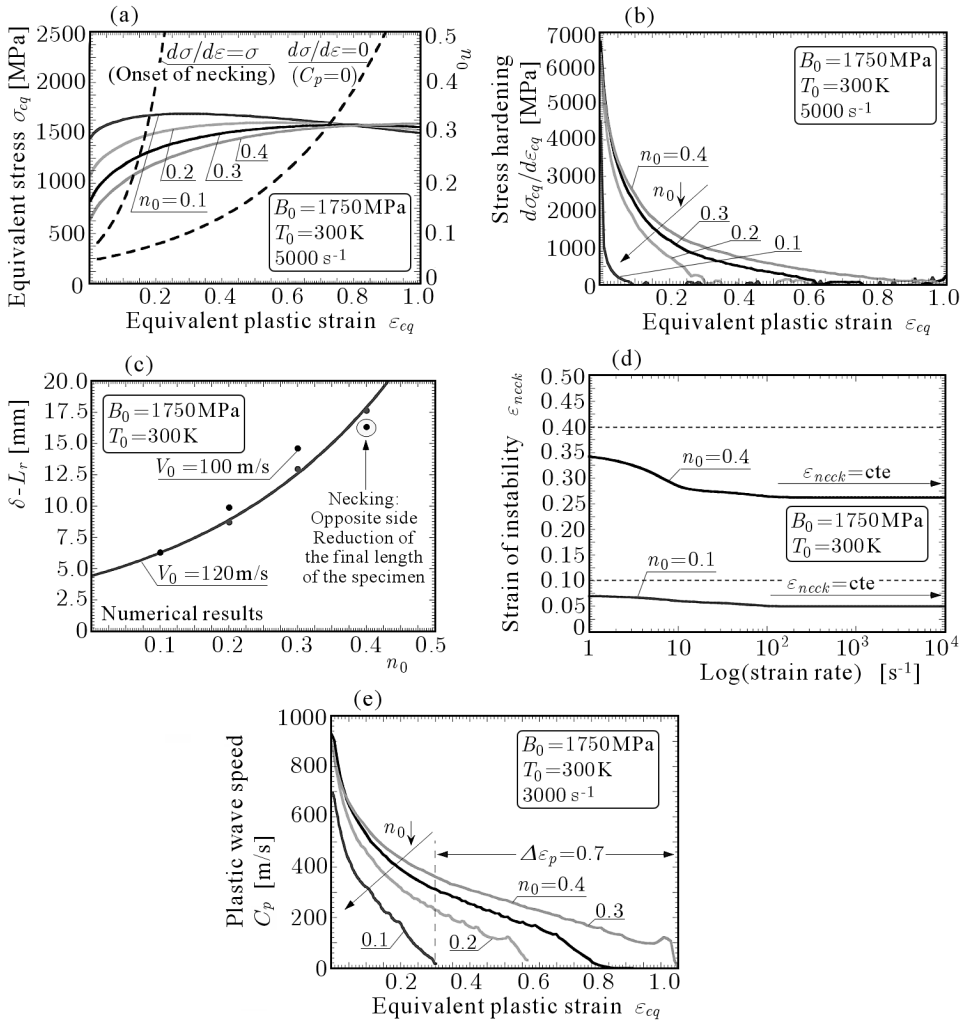


Fig. 5. Analytical predictions using RK model of (a) flow stress and (b) strain hardening along with plastic deformation for different values of n_0 at $T = 300\text{ K}$ and 5000 s^{-1} . (c) Elongation of the active part of the specimen with n_0 at $T = 300\text{ K}$ for $V_0 = 100\text{ m/s}$ and $V_0 = 120\text{ m/s}$. (d) Evolution of strain of instability along with strain rate. (e) Analytical predictions using RK model of the plastic wave speed with plastic strain for different values of n_0 at $T = 300\text{ K}$ and 3000 s^{-1}

The trapping of plastic deformation when the CIV is reached induces the loss of equilibrium in the specimen behaviour. In Fig. 9, the Input (*measured on the impacted end*) and the Output (*measured on the clamped end*) forces predicted by the numerical simulations for strain hardening exponents

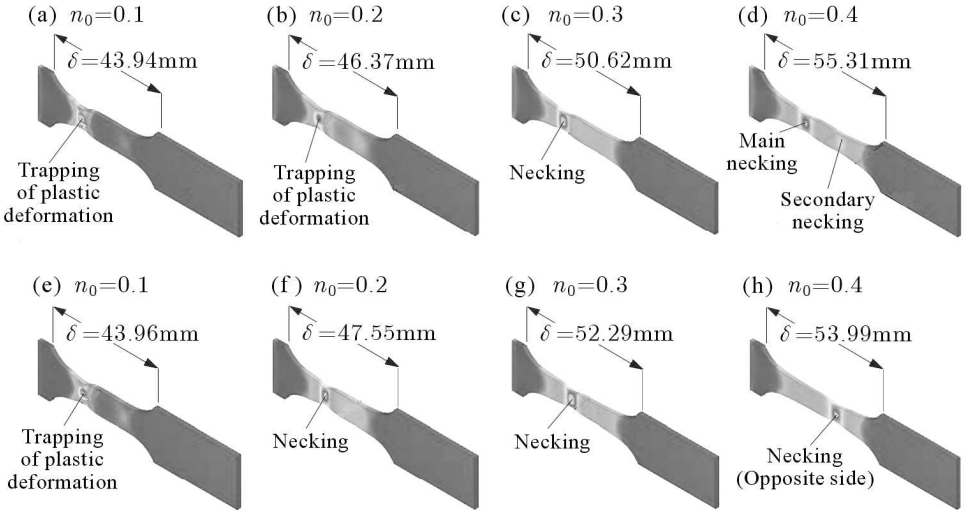


Fig. 6. Numerical estimation of the equivalent plastic strain contours for two impact velocities $V_0 = 120$ m/s (a)-(d) and $V_0 = 100$ m/s (e)-(h) and different strain hardening coefficients $n_0 = 0.1, 0.2, 0.3, 0.4$

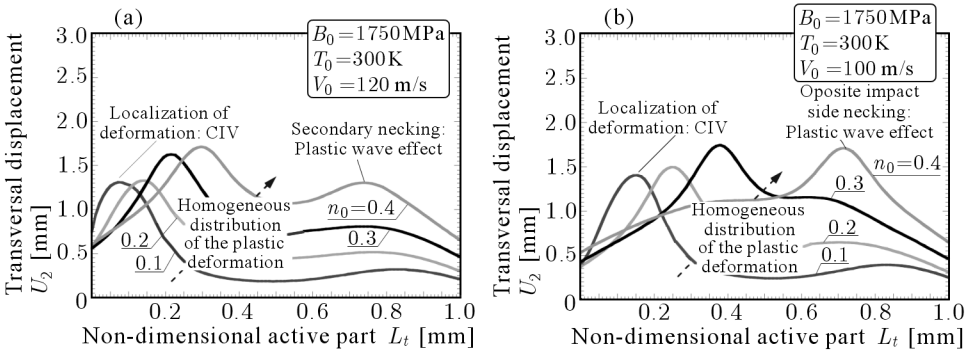


Fig. 7. Numerical estimation of the transversal displacement of the active part of the specimen for several values of n_0 ; (a) $V_0 = 120$ m/s, (b) $V_0 = 100$ m/s

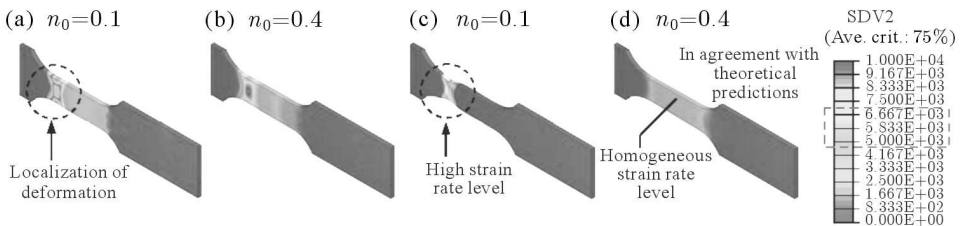


Fig. 8. Numerical estimation of the strain rate contours using different values of the strain hardening exponent n_0 in the case of $V_0 = 120$ m/s, 6000 s $^{-1}$, (a)-(b) $t = 28 \mu$ s, (c)-(d) $t = 52 \mu$ s

$n_0 = 0.1$ and $n_0 = 0.4$ and for the impact velocity $V_0 = 120$ m/s are compared. It can be observed that in the case of $n_0 = 0.1$ the equilibrium between both forces is never reached. On the contrary, in the case of $n_0 = 0.4$, once the inertia effects are overcome, the Input and Output forces meet for a determined force level. Plasticity acts as a filter to dissipate inertia effects.

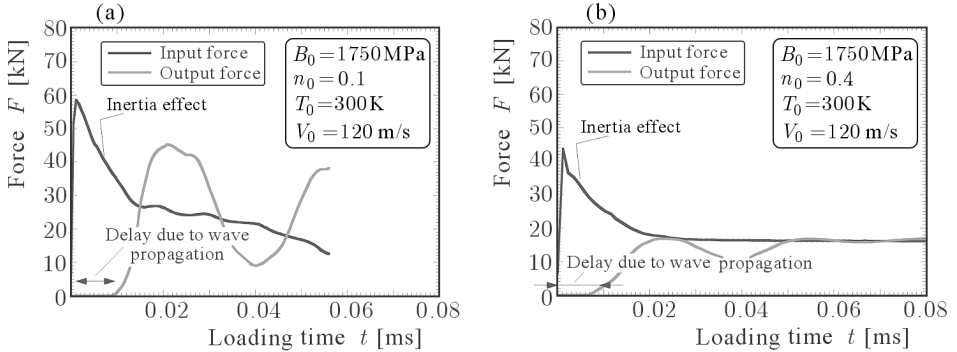


Fig. 9. Numerical estimation of the Input and Output forces for $V_0 = 120$ m/s; (a) $n_0 = 0.1$ – unstable behaviour (absence of equilibrium between Input and Output forces), (b) $n_0 = 0.4$ – stable behaviour (equilibrium between Input and Output forces)

According to the experimental results published in Mann (1936), Clark and Wood (1950), Klepaczko (1998b), the CIV may be measured by knowledge of the energy absorbed by the specimen during the impact. When the impact velocity is close to that corresponding to the CIV, the energy absorbed by the specimen is maximum. Then the plastic wave speed in adiabatic conditions near the impact end reaches zero $d\bar{\sigma}/d\bar{\varepsilon}_p = 0 \rightarrow C_p = 0$. Once the CIV is overcome, that energy suddenly decreases. Such behaviour is well described by the numerical simulations as shown in Fig. 10.

4.2. Effect of the modulus of plasticity B_0

The parameter B_0 rules the flow stress level of the material and its strain hardening. The flow stress level has an effect on the increase of temperature when the material behaves under adiabatic conditions of deformation since $\Delta T(\bar{\sigma}(\bar{\varepsilon}_p, \dot{\bar{\varepsilon}}_p, T))$. As the stress level increases, the material temperature does it as well. Moreover, it is known that the thermal softening accelerates the appearance of plastic instabilities and it reduces the strain hardening. Such an effect can be observed in Fig. 11a. Increasing the value of B_0 , the nec-

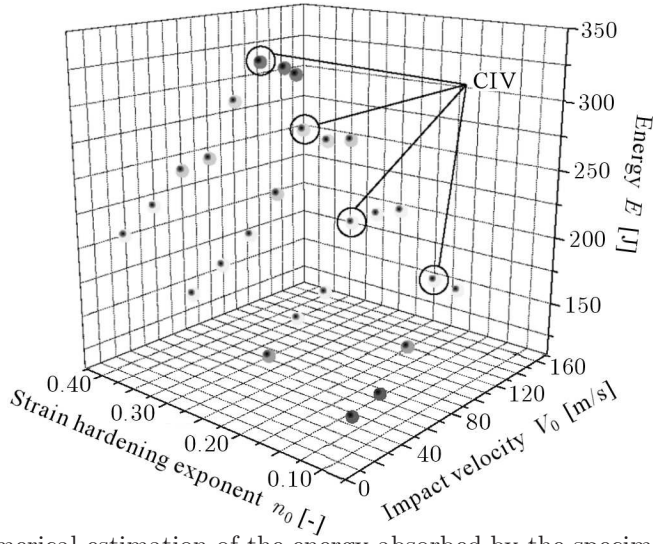


Fig. 10. Numerical estimation of the energy absorbed by the specimen along with n_0 and impact velocity

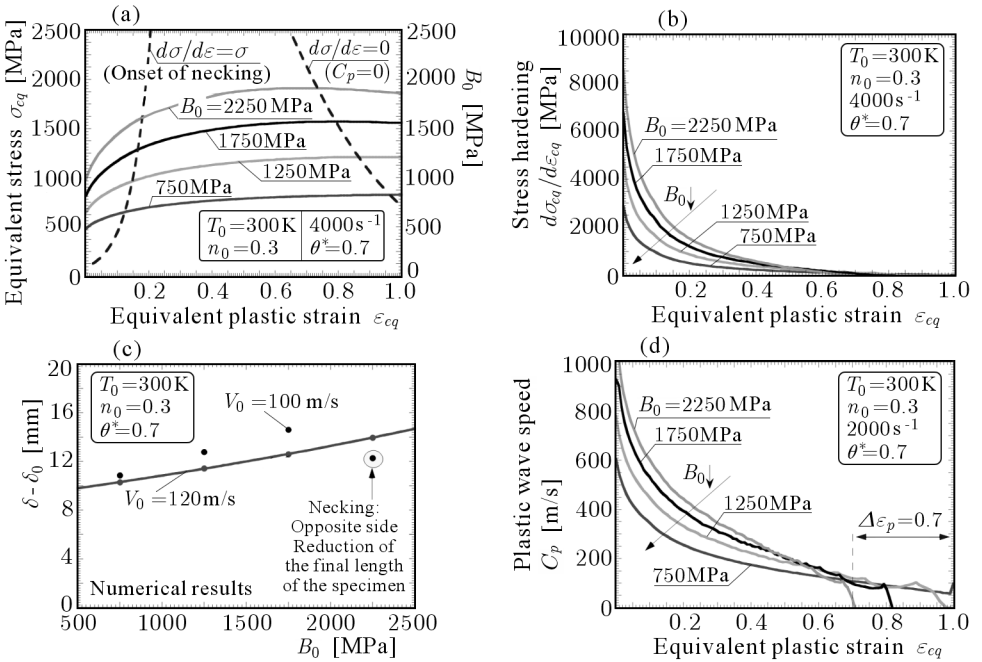


Fig. 11. Analytical predictions using RK model of (a) flow stress and (b) strain hardening along with plastic deformation for different values of B_0 at $T = 300\text{K}$ and 4000s^{-1} . (c) Displacement of the active part of the specimen with B_0 at $T = 300\text{K}$ for $V_0 = 100\text{m/s}$ and $V_0 = 120\text{m/s}$. (d) Analytical predictions using RK model of the plastic wave speed with plastic strain for different values of B_0 at $T = 300\text{K}$ and 2000s^{-1}

king condition $d\bar{\sigma}/d\bar{\varepsilon}_{neck} = \bar{\sigma}$ is delayed along with plastic strain. On the contrary, the condition of trapping of plastic waves $d\bar{\sigma}/d\bar{\varepsilon}_p = 0 \rightarrow C_p = 0$ is moved forwards. At low values of plastic deformation the strain hardening increases with B_0 (Fig. 11b) increasing ductility of the material (Fig. 11c). At high values of plastic deformation the strain hardening decreases with B_0 (Fig. 11d). Therefore, the parameter B_0 allows for uncoupling the effect that the necking condition and trapping of plastic waves condition has on the CIV.

In Fig. 12, the plastic strain contours estimated by numerical simulations for each value of B_0 considered and two different impact velocities, $V_0 = 120$ m/s and $V_0 = 100$ m/s are shown. The necking position is heavily dependent on B_0 , Fig. 12. It can be observed that the CIV is delayed with the increase of B_0 . For both impact velocities and $B_0 = 750$ MPa the necking takes place in the impacted end of the specimen, the CIV condition is fulfilled (Figs. 12-13). When $B_0 = 2250$ MPa, the necking takes place in the embedded side of the specimen for $V_0 = 120$ m/s and in the middle of the sample for $V_0 = 100$ m/s, see Figs. 12-13.

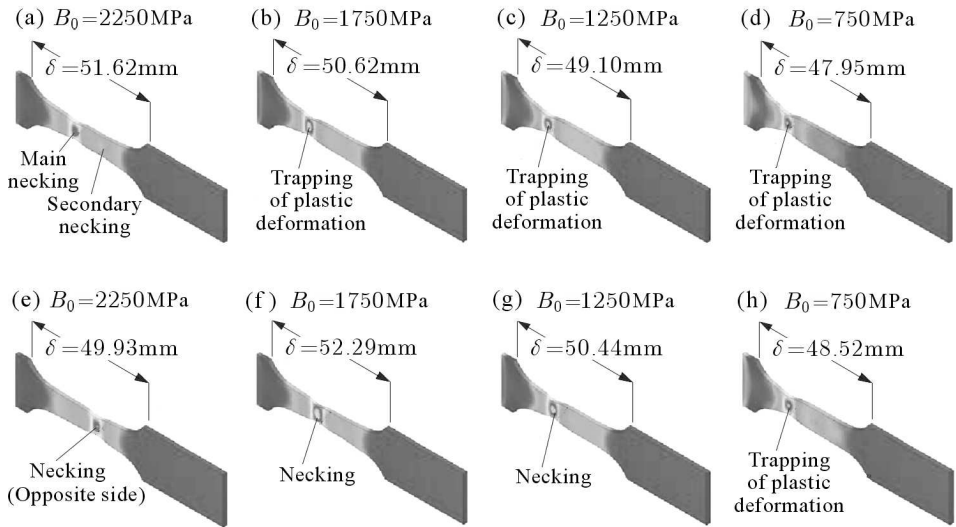


Fig. 12. Numerical estimation of the equivalent plastic strain contours using different values of the material constant B_0 in the case of $V_0 = 120$ m/s (a)-(d) and the case of $V_0 = 100$ m/s (e)-(h)

A comparison of the strain rate contours for two values of B_0 and two different impact velocities is shown in Fig. 14. In the case of $B_0 = 750$ MPa, the necking is already developed in the impacted end. In the case of

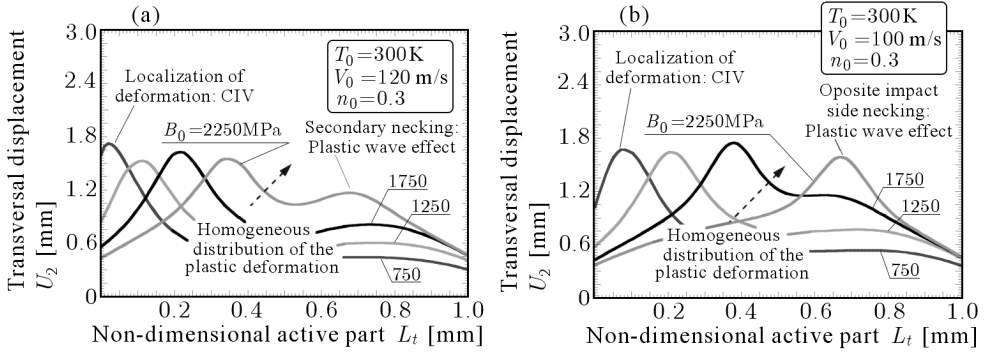


Fig. 13. Numerical estimation of the transverse displacement of the active part of the specimen for several values of the plasticity coefficient B_0 ; (a) $V_0 = 120$ m/s, (b) $V_0 = 100$ m/s

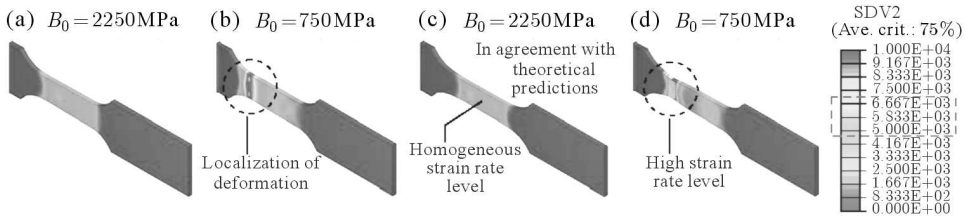


Fig. 14. Numerical estimation of the strain rate contours using different values of the material constant B_0 in the case of $V_0 = 120$ m/s, theoretical strain rate level = 6000 s^{-1} , (a)-(b) $t = 32 \mu\text{s}$, (c)-(d) $t = 76 \mu\text{s}$

$B_0 = 2250$ MPa, the strain rate level remains homogeneous and uniformly spreads all along the active part of the specimen.

Those differences in the sample behaviour can be observed comparing the Input and Output forces, see Fig. 15. In the case of $B_0 = 750$ MPa, both forces never reach equilibrium. A different trend is reported for $B_0 = 2250$ MPa. After the inertia effects are dissipated, both forces meet along with the loading time.

The estimation of energy absorbed by the specimen versus impact velocity for all the values of B_0 is shown in Fig. 16. It can be seen that the maximum energy absorbed by the specimen takes place for the greatest impact velocity when $B_0 = 2250$ MPa.

Next, the numerical estimations are compared with the analytical results provided by the analytical model developed by Klepaczko (2005).

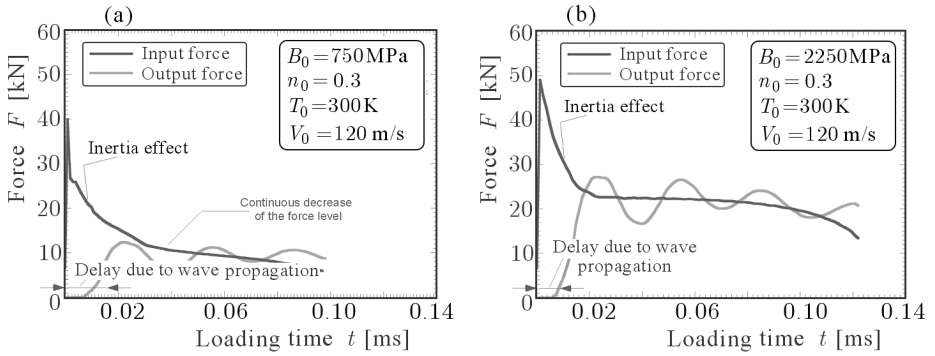


Fig. 15. Numerical estimation of the Input and Output forces for $V_0 = 120\text{ m/s}$; (a) $B_0 = 750\text{ MPa}$ – unstable behaviour (absence of equilibrium between Input and Output forces), (b) $B_0 = 2250\text{ MPa}$ – stable behaviour (equilibrium between Input and Output forces)

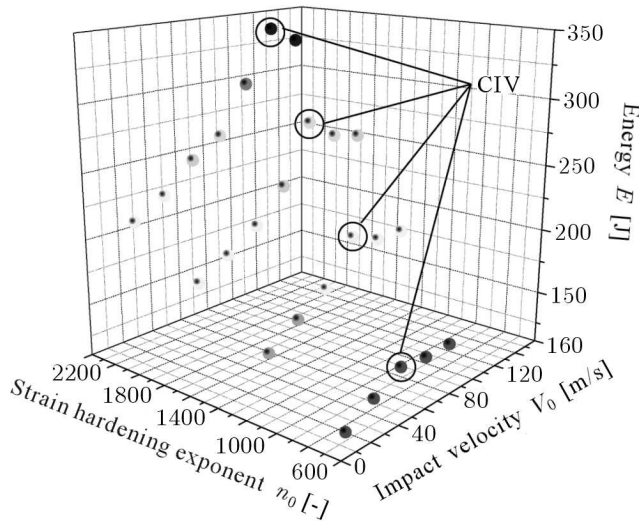


Fig. 16. Numerical estimation of the energy absorbed by the specimen versus B_0 and V_0

4.3. Analytical and numerical approach to CIV in tension

According to Klepaczko (2005), CIV can be obtained by integrating the wave celerity along strain. The expression for CIV can be split into two parts

$$\text{CIV} = \int_0^{\varepsilon_e} C_e(T) d\varepsilon + \int_{\varepsilon_e}^{\varepsilon_{pm}} C_p(\bar{\varepsilon}_p, \dot{\bar{\varepsilon}}_p, T) d\bar{\varepsilon}_p \quad (4.1)$$

The first term of Eq. (4.1) corresponds to the elastic range. In that term, $C_e(T)$ is the elastic wave celerity (*in a general case may be dependent on temperature*) and ε_e is the elastic deformation corresponding to the yield stress in a quasi-static condition. The second term corresponds to the plastic range. In that term, $C_p(\bar{\varepsilon}^p, \dot{\bar{\varepsilon}}^p, T)$ is the plastic wave celerity dependent on the strain hardening, strain rate and temperature. The upper limit of integration ε_{pm} may be considered as the plastic strain value corresponding to the instability criterion $d\bar{\sigma}/d\bar{\varepsilon}_{pm} = \bar{\sigma}$ (Considerere, 1885). Another possibility is to consider ε_{pm} as the plastic strain value corresponding to the trapping of plastic waves $C_p \rightarrow d\bar{\sigma}/d\bar{\varepsilon}_{pm} = 0$ (Klepaczko, 2005). However, the use of one or another possibility could strongly modify the analytical prediction of CIV for a determined material, see Fig. 17. Moreover, the analytical solution of Eq. (4.1) depends on the constitutive relation used to define the material behaviour since $C_p(\bar{\varepsilon}^p, \dot{\bar{\varepsilon}}^p, T) \propto \bar{\sigma}_{eq}(\bar{\varepsilon}^p, \dot{\bar{\varepsilon}}^p, T)$. In addition, the thermal coupling must be taken into account (Klepaczko, 2005) and, then, the increase of temperature becomes dependent on plastic deformation $dT/d\bar{\varepsilon}^p \neq 0$.

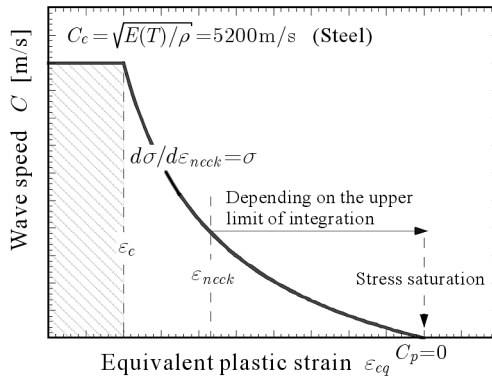


Fig. 17. Schematic representation of the wave speed along plastic strain for a given strain rate and temperature levels. Influence of the upper limit of integration ε_{pm} on the CIV value

Next, the results of the CIV value obtained by Eq. (4.1), are compared with the values obtained from the numerical simulations.

In order to get an analytical solution to Eq. (4.1), the following procedure has been followed:

- The elastic contribution to CIV is calculated to obtain the stress level corresponding to $\bar{\varepsilon}^p = 0$ from the analytical predictions of the RK model. Then, by application of Hook's law the upper limit of integration ε_e is obtained. Assuming a constant celerity of the plastic waves $C_e \approx 5200$ m/s, the elastic contribution can be obtained.

- The contribution of the plastic range is calculated using the analytical predictions of the RK constitutive relation. Both conditions discussed previously

– *Condition 1*: $d\bar{\sigma}/d\bar{\varepsilon}_{pm} = \bar{\sigma}$

– *Condition 2*: $d\bar{\sigma}/d\bar{\varepsilon}_{pm} = 0$

are considered to calculate the upper limit of integration ε_{pm} .

The analytical and numerical results obtained for the CIV are listed in Tables 3-4.

Table 3. Analytical estimations of CIV and comparison with the numerical results

	B_0 [MPa]			
	2250	1750	1250	750
<i>Condition 1</i>	144 m/s	121 m/s	101 m/s	69 m/s
<i>Condition 2</i>	269 m/s	255 m/s	233 m/s	190 m/s
Numerical	130 m/s	110 m/s	90 m/s	70 m/s

Table 4. Analytical estimations of CIV and comparison with the numerical results

	$n_0 = 0.4$	$n_0 = 0.3$	$n_0 = 0.2$	$n_0 = 0.1$
<i>Condition 1</i>	146 m/s	121 m/s	102 m/s	62 m/s
<i>Condition 2</i>	317 m/s	255 m/s	188 m/s	118 m/s
Numerical	130 m/s	110 m/s	90 m/s	80 m/s

It can be observed that *Condition 1* provides the results which better fit the numerical estimations. Although the phenomenon of CIV is governed by *Condition 2*, the value of CIV seems to be ruled by the condition of instability, *Condition 1*. Such a conclusion allows for optimization of materials used under dynamic applications which, eventually, may be susceptible to the appearance of instabilities. Some examples are those materials used for constructing ballistic armours or crash-box structures. According to the results reported in this document, metals showing low stress level but high strain hardening seem to be more suitable for absorbing energy instead of materials showing a high flow stress but a reduced strain hardening.

5. Concluding and remarks

In this paper, the influence of strain hardening on CIV in tension has been examined using numerical simulations. The material behaviour has been defined by means of the constitutive description due to Rusinek and Klepaczko. The numerical simulations have been conducted for a wide range of impact velocities up to that corresponding to the CIV. Two parameters of the strain hardening formulation of the model have been varied in order to study their influence on the CIV value. The numerical predictions of CIV have been compared with the analytical results. The following main conclusions are obtained from the analysis:

- Strain hardening shows great influence on CIV of materials. The CIV value strongly increases with strain hardening. A strain hardening increase delays the appearance of plastic instabilities augmenting ductility of the material. An increase of the yield stress leads to a decrease of the energy absorbed by materials due to adiabatic heating. Thermal softening is more important as the flow stress level increases, it reduces the CIV value.
- Although the CIV phenomenon is founded on the trapping of plastic waves, the CIV value seems to be ruled by the condition of instability. The analytical approach developed by Klepaczko (2005) allows for defining such behaviour and provides results according to numerical simulations.

References

1. ARIAS A., RODRIGUEZ-MARTINEZ J.A., RUSINEK A., 2008, Numerical simulations of impact behaviour of thin steel to cylindrical, conical and hemispherical non-deformable projectiles, *Eng. Fract. Mech.*, **75**, 1635-1656
2. BERBENNI S., FAVIER V., LEMOINE X., BERVEILLER N., 2004, Micromechanical modelling of the elastic-viscoplastic behaviour of polycrystalline steels having different microstructures, *Mat. Sci. and Eng.*, **372**, 128-136
3. BORVIK T., LANGSETH M., HOPERSTAD O.S., MALO K.A., 2002, Perforation of 12 mm thick steel plates by 20 mm diameter projectiles with flat, hemispherical and conical noses. Part I: Experimental study, *Int. J. Impact Eng.*, **27**, 1, 19-35

4. CLARK D.S., WOOD D.S., 1950, The influence of specimen dimension and shape on the results in tension impact testing, *Proc. ASTM*, **50**, 577
5. CONSIDERE M., 1885, L'emploi du fer de l'acier dans les constructions, *Memoire no 34. Annales des Ponts et Chaussées*, Paris, 574-575
6. FORRESTAL M.J., PIEKUTOWSKI A.J., 2000, Penetration experiments with 6061-T6511aluminum targets and spherical-nose steel projectiles at striking velocities between 0.5 and 3.0 km/s, *Int. J. Impact Eng.*, **24**, 57-67
7. HU X., DAEHN G.S., 1996, Effect of velocity on flow localization in tension, *Acta Mater.*, **44**, 1021-1033
8. KLEPACZKO J.R., 1975, Thermally activated flow and strain rate history effects for some polycrystalline FCC metals, *Mater. Sci. Eng.*, **18**, 121-135
9. KLEPACZKO J.R., 1987, A practical stress-strain-strain rate-temperature constitutive relation of the power form, *J. Mech. Working Technol.*, **15**, 143-165
10. KLEPACZKO J.R., 1998a, A general approach to rate sensitivity and constitutive modeling of FCC and BCC metals, In: *Impact: Effects of Fast Transient Loadings*, A.A. Balkema, Rotterdam, 3-35
11. KLEPACZKO J.R., 1998b, Remarks on impact shearing, *J. Mech. Phys. Solids.*, **35**, 1028-1042
12. KLEPACZKO J.R., 2005, Review on critical impact velocities in tension and shear, *Int. J. Impact Eng.*, **32**, 188-209
13. KLEPACZKO J.R., 2006, Dynamic instabilities and failures in impact tension, compression and shear, *Conference Information: 8th International Conference on Mechanical and Physical Behaviour of Materials under Dynamic Loading*, Dijon, France, *Journal of Physique IV*, **134**, 857-867
14. KLEPACZKO J.R., KLOSAK M., 1999, Numerical study of the critical impact velocity in shear, *European Journal of Mechanics A-Solids*, **1**, 93-113
15. KLEPACZKO J.R., RUSINEK A., RODRÍGUEZ-MARTÍNEZ J.A., PEŁCHERSKI R.B., ARIAS A., 2009, Modeling of thermo-viscoplastic behaviour of DH-36 and Weldox 460-E structural steels at wide ranges of strain rates and temperatures, comparison of constitutive relations for impact problems, *Mechanics of Materials*, **41**, 599-621
16. KLOSAK M., LODYGOWSKI T., KLEPACZKO J.R., 2001, Remarks on numerical estimation of the critical impact velocity in shear, *CAMES*, **8**, 579-593
17. KOCKS U.F., ARGON A.S., ASHBY M.F., 1975, Thermodynamics and kinetics of slip, In: *Progress in Materials Science*, Chalmers B., Christian J.W., Massalski T.B. (Edit.), **19**, Pergamon Press, Oxford
18. MANN H.C., 1936, High-velocity tension-impact tests, *Proc. ASTM*, **36**, 85

19. NEMAT-NASSER S., GUO W.G., 2003, Thermomechanical response of DH-36 structural steel over a wide range of strain rates and temperatures, *Mech. Mat.*, **35**, 1023-1047
20. OUSSOUADDI O., KLEPACZKO J.R., 1991, Analysis of transition between the isothermal and adiabatic deformation in the case of torsion of a tube, *Journal de Physique IV*, **1**, 323-334 [in French]
21. RUSINEK A., KLEPACZKO J.R., 2001, Shear testing of sheet steel at wide range of strain rates and a constitutive relation with strain-rate and temperature dependence of the flow stress, *Int. J. Plasticity*, **17**, 87-115
22. RUSINEK A., KLEPACZKO J.R., 2003, Impact tension of sheet metals – effect of initial specimen length, *7th International Conference on Mechanical and Physical Behaviour of Materials Under Dynamic Loading*, Oporto, *Journal of Physique IV*, **10**, 329-334
23. RUSINEK A., RODRÍGUEZ-MARTÍNEZ J.A., KLEPACZKO J.R., PECHERSKI R.B., 2009, Analysis of thermo-visco-plastic behaviour of six high strength steels, *J. Mater. Design*, **30**, 1748-1761
24. RUSINEK A., ZAERA R., 2007, Finite element simulation of steel ring fragmentation under radial expansion, *Int. J. Impact Eng.*, **34**, 799-822
25. RUSINEK A., ZAERA R., FORQUIN P., KLEPACZKO J.R., 2008, Effect of plastic deformation and boundary conditions combined with elastic wave propagation on the collapse site of a crash box, *Thin-Walled Structures*, **46**, 1143-1163
26. RUSINEK A., ZAERA R., KLEPACZKO J.R., 2007, Constitutive relations in 3-D for a wide range of strain rates and temperatures – Application to mild steels, *Int. J. Solids Struct.*, **44**, 5611-5634
27. RUSINEK A., ZAERA R., KLEPACZKO J.R., CHERIGUENE R., 2005, Analysis of inertia and scale effects on dynamic neck formation during tension of sheet steel, *Acta Mater.*, **53**, 5387-5400
28. SEEGER A., 1957, The mechanism of glide and work-hardening in face-centered cubic and hexagonal close-packed metal, In: *Dislocations and Mechanical Properties of Crystals*, J. Wiley, New York
29. ZAERA R., FERNANDEZ-SAEZ J., 2006, An implicit consistent algorithm for the integration of thermoviscoplastic constitutive equations in adiabatic conditions and finite deformations, *Int. J. Solids Struct.*, **43**, 1594-1612
30. ZUKAS J.A., SCHEFFLER D.R., 2000, Practical aspects of numerical simulations of dynamic events: effects of meshing, *Int. J. Impact Eng.*, **24**, 925-945

Zależność między umocnieniem odkształceniowym stali a krytyczną prędkością uderzenia przy rozciąganiu

Streszczenie

Praca przedstawia numeryczną analizę wpływu umocnienia odkształceniowego na krytyczną prędkość uderzenia (CIV) przy rozciąganiu. W symulacjach zastosowano oprogramowanie ABAQUS/Explicit oparte na metodzie elementów skończonych. Obliczeń dokonano dla dynamicznych obciążeń rozciągających w szerokim zakresie prędkości uderzenia aż do osiągnięcia wartości krytycznej (CIV). Do opisu materiału próbki użyto równań konstytutywnych modeli Rusinka-Klepaczki. Podczas analizy zmieniano parametry umocnienia odkształceniowego opisanego tym modelem. Wyniki symulacji numerycznych porównano z analitycznym opisem CIV zaproponowanym przez Klepaczkę (2005). Uzyskano zadawalającą zgodność pomiędzy symulacją a teorią. Przedstawiona analiza przyczynia się do lepszego zrozumienia zjawisk odpowiedzialnych za powstawanie krytycznej prędkości uderzenia (CIV).

Manuscript received April 21, 2009; accepted for print May 23, 2009